Journal Name

ARTICLE

Two-way Vapochromism of a Luminescent Platinum(II) Complex with Phosphonic-acid-functionalized Bipyridine Ligand

Received 00th January 20xx,
Accepted 00th January 20xx

DOI: 10.1039/x0xx00000x

www.rsc.org/

Atsushi Kobayashi,* Naotaka Yamamoto, Yasuhiro Shigeta, Masaki Yoshida and Masako Kato*

A luminescent Pt(II) complex [Pt(CN)$_2$(H$_2$dpbpy)] (**1P**; H$_2$dpbpy = 2,2'-bipyridine-4,4'-diphosphonic acid) bearing a phosphonic-acid-functionalized bipyridine ligand was successfully synthesized and its unique two-way vapochromic behaviour investigated. X-ray structure analyses of both the anhydrous **1P** and penta-hydrated **1P·5H$_2$O** phases clearly reveal the activation of intermolecular Pt···Pt interactions through the adsorption of water vapour. Emission spectroscopy reveals that the penta-hydrated **1P·5H$_2$O** complex exhibits an orange emission at 585 nm that shifts in two directions, to a blue-green emission at 469 nm by drying at 100 °C or to a red emission at 701 nm by drying under vacuum at room temperature. Thermogravimetric analyses and powder X-ray diffraction studies clearly reveal that anhydrous **1P**, with negligible intermolecular Pt···Pt interactions, is formed by drying at 100 °C whereas the monohydrate **1P·H$_2$O** phase, with effective Pt···Pt interactions, is formed by drying under vacuum.

Introduction

Vapochromism, chromism induced by reversible vapour adsorption/desorption, has received increasing attention recently, not only because of is promising application to solid-state chemical sensors for toxic gases and vapours, but also because of its potential in applications such as molecule-based switches and devices.[1-2] From the pioneering work by Mann and co-workers in 1995,[3] many vapochromic materials have been developed. These extensive works revealed that there are several requirements that need to be satisfied when designing vapochromic materials. The first is lattice flexibility required for the adsorption of vapour molecules into the lattice framework. From this viewpoint, porous materials such as metal-organic frameworks and related compounds are promising candidates and several interesting materials have been reported to date.[4-14] The second requirement is the availability of a suitable chromophore for the direct naked-eye detection of vapour molecules or vapour-adsorption-induced lattice transformations. To satisfy this second requirement, various approaches have been explored. A typical approach involves the use of chromophores such as Pt(II) and Au(I) complexes.[15-22] These complexes can detect small lattice distortions induced by the adsorption of vapour through highly sensitive electronic transitions involving intermolecular metallophilic interactions. Other promising approaches recently developed involve the use of host-guest interactions between the adsorbing material and vapour molecules[23-28] or the use of ligand substitution reactions at metal centres.[29-37] Most of the vapochromic behaviour reported so far is essentially based on the colour differences between vapour-adsorbed and vapour-released phases. Although many vapochromic materials have been reported to date, there are few examples that exhibit switching vapochromic behaviour.[38] The development of such switching functionalities in vapochromic materials is an important step toward the design of smart chemical sensors that can not only detect toxic gas/vapour, but also other environmental parameters such as temperature and pressure, among others.

Our recent attention has focused on exploring the additional functionalities of vapochromic Pt(II) complexes through intermolecular hydrogen-bonding interactions.[39-41] Hydrogen bonds are well-known flexible and directional intermolecular interactions.[42-43] These characteristics are advantageous from the viewpoint of crystal engineering. For example, Eisenberg *et al.* reported single-crystal to single-crystal transformations in a vapochromic Pt(II) complex with intermolecular hydrogen-bonding interactions constructed through amide groups.[44-45] We also reported the unique "shape-memory" vapochromism of the porous Pt(II) complex, [Pt(CN)$_2$(H$_2$dcbpy)] (**1C**; Scheme 1; H$_2$dcbpy = 2,2'-bipyridine-4,4'-dicarboxylic acid) built through intermolecular interactions between carboxylic acids and cyanide groups.[39] Although single-proton-donating and accepting groups, like carboxylic acids and amides, have been widely investigated to date,[46-51] the double-proton-donating phosphonic acid group has scarcely been used in vapochromic Pt(II) complexes; its two-proton-donating ability enables the

[a] *Department of Chemistry, Faculty of Science, Hokkaido University, North-10 West-8, Kita-ku, Sapporo, Hokkaido 060-0810, Japan; e-mail: akoba@sci.hokudai.ac.jp (A.K.), mkato@sci.hokudai.ac.jp (M.K.)*

† Electronic Supplementary Information (ESI) available: X-Ray crystallographic data in CIF format; UV-Vis spectra of **1P** in aqueous solution, Changes of emission spectra of **1P-H** and **1P-V** under exposure to water vapour, Temperature dependence of the PXRD pattern of **1P-V**, water vapour adsorption isotherms, thermogravimetric analysis and IR spectra of **1P-H, 1P-V**. See DOI: 10.1039/x0xx00000x

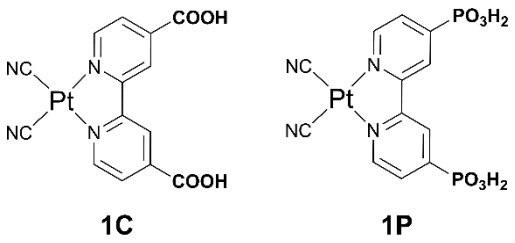

1C 1P

Scheme 1. Molecular structures of the Pt(II) complexes.

design of a variety of crystalline phases with different protonated states. In this work, we report the synthesis and vapochromic behaviour of the luminescent Pt(II) complex [Pt(CN)$_2$(H$_2$dpbpy)] (**1P**; Scheme 1; H$_2$dpbpy = 2,2'-bipyridine-4,4'-diphosphonic acid) bearing a phosphonic-acid-functionalized bipyridine ligand and demonstrate that the penta-hydrated form of **1P** exhibits unique two-way vapochromic behaviour triggered by two different drying conditions.

Experimental Section

Synthetic procedures.

Caution! *Although we experienced no difficulties, most of the chemicals used in this study are potentially harmful and should be used in small quantities and handled with care in a fume hood.* All commercially available starting materials were used without purification. The starting compounds, Pt(CN)$_2$ and H$_4$dpbpy, were synthesized following literature procedures.[52,53]

Synthesis of [Pt(CN)$_2$(H$_4$dpbpy)]·5H$_2$O (1P·5H$_2$O). Pt(CN)$_2$ (304 mg, 1.23 mmol) and H$_4$dpbpy (384 mg, 1.21 mmol) powders were suspended in aqueous ammonia (28%, 120 mL) and refluxed for 2 d. The reaction mixture was filtered to remove unreacted starting material, after which 0.018 M aqueous Ca(OH)$_2$ (500 mL) was added to the filtrate. The red precipitate was collected by filtration and then dissolved in dilute aqueous HCl (3M, 100 mL). After reducing the amount of solvent to ~30 mL by rotary evaporation, a bluish-purple precipitate formed upon the addition of conc. HCl (110 mL) to the solution, which was collected by filtration. This bluish-purple powder was then dissolved in a minimum amount of water and acetone vapour deposition was carried out at room temperature for several days to afford orange crystals of **1P·5H$_2$O**. A single crystal was used for X-ray crystallographic studies. Yield: 303 mg (464 μmol, 38%). Elemental analysis calcd for C$_{12}$H$_{10}$N$_4$O$_6$P$_2$Pt·5H$_2$O: C 22.06, H 3.09, N 8.58. Found: C 22.01, H 2.85, N 8.63. ^{1}H NMR (DMSO-d^6, 298 K) δ 8.10 (ddd, 2H), 8.68 (d, 2H), 9.26 (dd, 2H).

Synthesis of [Pt(CN)$_2$(H$_4$dpbpy)] (1P). A powder sample of **1P·5H$_2$O** (32.5 mg, 49.8 mmol) was dissolved in a small amount of water (0.5 mL) and ethanol vapour deposition was performed at 50 °C for two weeks to afford pale yellow crystals of **1P.** Yield: 11.0 mg (19.5 mmol, 39%). A single crystal was used for X-ray crystallographic studies. Elemental analysis, calcd. for C$_{12}$H$_{10}$N$_4$O$_6$P$_2$Pt: C 25.59, H 1.74, N 9.95. Found: C 25.46, H 1.59, N 9.77.

X-ray Crystallographic Studies.

Single-crystal X-ray diffraction experiments were performed on a Rigaku Mercury CCD diffractometer with graphite-monochromated Mo *K*α radiation (λ = 0.71069 Å) and a rotating anode generator or a Rigaku AFC-11 diffractometer with a Mercury CCD area detector at beamline PF-AR NW2A at the Photon Factory, KEK, Japan. The wavelength of synchrotron X-rays was 0.6889(1) Å. A crystal was mounted on a loop using paraffin oil. The crystal was then cooled using a N$_2$-flow temperature controller. Diffraction data were collected and processed using the CrysAlisPro or CrystalClear programs.[54] The structures were solved by direct methods using SIR-2004 or SIR-2014,[55] and then refined by full-matrix least-squares methods using SHELXL-2013.[56] All non-hydrogen atoms were refined anisotropically, and hydrogen atoms were refined using a riding model. All calculations were performed using CrystalStructure, a crystallographic software package.[57] The crystallographic data are summarized in Table 1 and full crystallographic data have been deposited with the Cambridge Crystallographic Data Centre (CCDC 1584034, 1584164, 1812551).

Table 1. Crystal parameters and refinement data.

Complex	**1P**	**1P·5H$_2$O**	
T / K	200(1)	200(1)	83(1)
Formula	C$_{12}$H$_{10}$N$_4$O$_6$P$_2$Pt	C$_{12}$H$_{10}$N$_4$O$_6$P$_2$Pt·5H$_2$O	
Formula weight	563.27	653.35	
Crystal System	Monoclinic	Triclinic	
Space group	*I*2/*a*	*P*-1	
a / Å	8.8029(1)	6.718(2)	6.659(1)
b / Å	10.7829(2)	11.773(3)	11.753(2)
c / Å	17.1646(2)	13.485(4)	13.471(3)
α / deg	90	76.90(1)	77.029(9)
β / deg	96.438(1)	81.12(1)	81.16(1)
γ / deg	90	78.11(1)	78.25(1)
V / Å^3	1619.01(4)	1010.0(5)	999.4(4)
Z	4	2	
D_{cal} / g·cm^{-3}	2.311	2.148	2.171
Reflections collected	5757	15735	16901
Unique reflections	1650	5160	5542
GOF	1.144	1.209	1.253
R_{int}	0.0148	0.0466	0.0346
R_1(I) [a]	0.0158	0.0326	0.0288
wR_2 [b]	0.0417	0.1087	0.0996

[a] $R_1 = \Sigma||F_o| - |F_c||/\Sigma|F_o|$. [b] $wR_2 = [\Sigma w(F_o^2 - F_c^2)/\Sigma w(F_o)^2]^{1/2}$, $w = [\sigma_c^2(F_o^2) + (xP)^2 + yP]^{-1}$, $P = (F_o^2 + 2F_c^2)/3$.

Measurements.

Elemental analyses were performed at the Analysis Center of Hokkaido University. ^{1}H NMR spectra were obtained using a JEOL EX270 NMR spectrometer. Powder X-ray diffraction (PXRD) measurements were conducted using a Rigaku SPD diffractometer at the BL-8B beamline of the Photon Factory, KEK, Japan, or a Bruker D8 Advance diffractometer equipped with a graphite monochromator using Cu Kα radiation and a one-dimensional LinxEye detector. The synchrotron X-ray wavelength was 0.8857(1) Å. UV-vis spectra were obtained in solution using a Shimadzu UV-2400PC spectrophotometer.

Luminescence and IR spectra at room temperature were obtained using a JASCO FP-6600 spectrometer and a JASCO FT/IR spectrometer, respectively. Luminescence spectra at 77 K were recorded on a JASCO FP-8500 spectrofluorometer. The emission decay curves were measured using a Quantaurus-Tau C11367 (Hamamatsu Photonics K. K.) excited by a UV LED light source (λ_{ex} = 280 nm). Vapour-adsorption isotherms were obtained using a BELSORP-max instrument. Thermogravimetric and differential thermal analyses were performed using a Rigaku ThermoEvo TG8120 analyser.

Results and Discussion

Crystal Structures.

Fig. 1 displays the crystal structure of penta-hydrated **1P·5H$_2$O** at 200 K. Selected bond distances and angles are listed in Table S1 in the ESI. The central Pt(II) ion has adopted the square-planar coordination geometry typically found in Pt(II) complexes. Its four coordination sites are occupied by two N atoms of the phosphonate-functionalized bpy ligand and two cyanide C atoms. The bond distances around the Pt(II) ion (1.95(1) Å and 2.05(1) Å for the Pt-C and Pt-N bonds, respectively) are comparable with those in **1C**, the analogous carboxylic-acid-functionalized dicyanide-Pt(II) complex [Pt(CN)$_2$(H$_2$dcbpy)] (Table S1). The comparable distances around the Pt(II) ions observed in **1P** and **1C** suggests that substitution of the carboxylic acid groups at the 4,4′-positions of the bpy ligand for phosphonic acid groups hardly affects the electronic state of the Pt(II) ion. Two of the three P-O bond distances around the P1 atom (P1-O1 and P1-O2) are relatively longer (> 1.5 Å) than the other (P1-O3), whereas one bond distance (P2-O5) is intermediate between the other two. Although we tentatively assigned this phosphonic acid group to be fully protonated, it may be singly deprotonated to form the monoanionic complex, i.e., [Pt(CN)$_2$(H$_3$dpbpy)]$^-$. However, in that case, no counter cation was found in the crystal structure of **1P·5H$_2$O**, suggesting that one of the five hydrated water molecules (O7-O11) is protonated. On the basis of the significantly short O-H···O hydrogen-bond distance between O8 and O9 (2.502(12) Å, Table S2), either oxygen atom could be protonated. This conclusion is also supported by elemental analysis results that are in good agreement with the calculated data for penta-hydrated **1P·5H$_2$O** (see Experimental section). As shown in Fig. 1(b), both the phosphonic acid groups are hydrogen-bonded to the O atoms of water molecules and an O atom of the same functional group in an adjacent molecule, resulting in the penta-hydrated structure of **1P·5H$_2$O**. Although most of the atoms of this complex are located in the square-planar coordination plane of the Pt(II) ion, the O atoms of the phosphonic acid groups deviate from this plane due to the sp^3 electronic configuration of the P atom. Since these almost-planar molecules are stacked along the *a* axis (Fig. 1(a)), the intermolecular Pt···Pt distances (ca. 3.37 Å) are shorter than the sum of the van der Waals radii of two Pt atoms (3.50 Å), indicating the existence of effective intermolecular Pt···Pt interactions in the stacked columnar structure. These intermolecular Pt···Pt distances are longer by about 0.12 Å

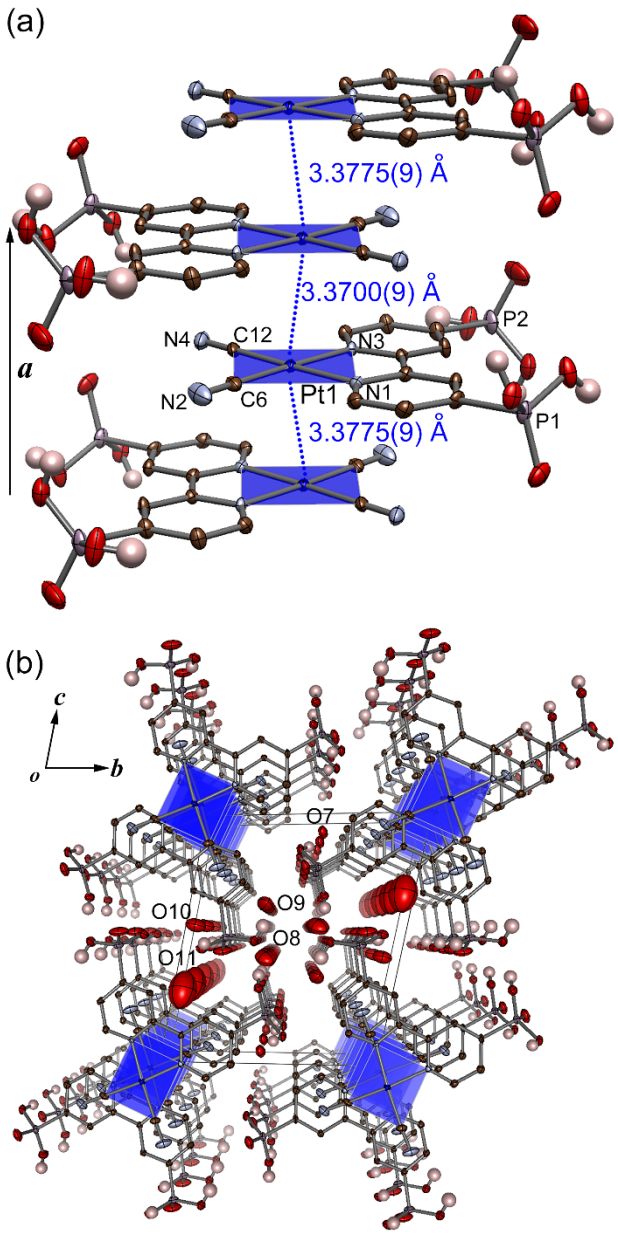

Fig. 1. (a) Stacking and (b) packing structures of **1P·5H$_2$O** at 200 K. The coordination planes of the Pt(II) ions are shown in blue. The blue, purple, brown, light-blue, and red ellipsoids represent Pt, P, C, N, and O atoms, respectively. The H atoms bonded to the O atoms of the phosphonic acid groups are shown in pink, while the others have been omitted for clarity. Displacement parameters are drawn at the 50% probability level.

than those in complex **1C** despite their comparable Pt···Pt···Pt stacking angles of around 170°, which is probably due to the larger steric hindrance of the phosphonic acid group compared to the carboxylic acid. The most remarkable difference between complexes **1P·5H$_2$O** and **1C** is the packing structure; complex **1C,** with two carboxyl groups forms a porous two-dimensional hydrogen-bonded network structure as reported previously,[39,41] whereas no porous channel is found in the phosphonic-acid-functionalized complex **1P·5H$_2$O**. At 83 K,

almost the identical crystal structure with slightly shrank lattice parameters to that at 200 K was confirmed (see Table 1).

The anhydrous form **1P** was obtained by ethanol vapour deposition to an aqueous solution of the penta-hydrated **1P·5H$_2$O** complex; Fig. 2 displays the crystal structure of **1P**. Half of the molecule was found to be crystallographically independent due to the higher symmetry of **1P** over **1P·5H$_2$O**. The bond distances and angles around the Pt(II) ions in **1P** are comparable to those in **1P·5H$_2$O** (Table S1), indicating that the removal of the water molecules from the crystal has a negligible effect on the electronic states of the Pt(II) ions. The most noteworthy differences between **1P** and **1P·5H$_2$O** are the intramolecular P-O bond distances of the phosphonic acid groups; only two of the six P-O bonds in **1P** are shorter than 1.5 Å, suggesting that two phosphonic acid groups of the dpbpy ligands are fully protonated. This doubly protonated phosphonic acid group forms two different intermolecular hydrogen bonds; an O1-H···O3 bond (2.494(4) Å) along the *a* axis, and an O2-H···N2 bond (2.619(4) Å) that tightly connects two adjacent molecules along the *b* axis. The hydrogen bonds formed in the crystal structure of **1P** are quite different to those formed in **1P·5H$_2$O**, leading to a completely different packing structure to that of **1P·5H$_2$O** or **1C**. As shown in Fig. 2(a), the planar Pt(II) molecule forms a zigzag-type stacked structure along the *a* axis. In this stacked structure, the intermolecular Pt···Pt distances exceed 4.5 Å, indicating that intermolecular Pt···Pt interactions are negligible. The completely different packing structures observed for **1P** and **1P·5H$_2$O** are possibly responsible for the colours of these crystals; **1P·5H$_2$O** is orange in colour, while **1P** is pale yellow. These details are discussed in the following section.

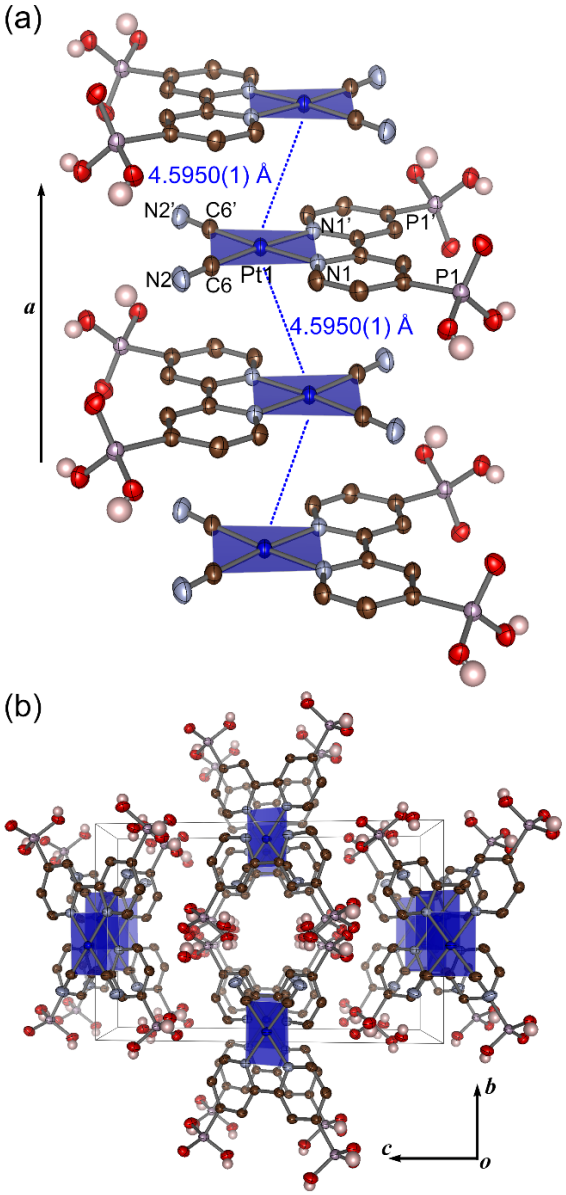

Fig. 2. (a) Stacking and (b) packing structures of **1P**. The coordination planes of the Pt(II) ions are shown in blue. The blue, purple, brown, light-blue, and red ellipsoids represent Pt, P, C, N, and O atoms, respectively. The H atoms bonded to the O atoms of the phosphonic acid groups are shown in pink, while the others have been omitted for clarity. Displacement parameters are drawn at the 50% probability level.

Two-way vapochromic behaviour.

As mentioned in the Introduction, the carboxylic acid analogue **1C** exhibited an interesting "shape-memory" vapochromic response that has its origins in its unique porous structure.[41] This finding motivated us to investigate the vapochromic behaviour of the phosphonic-acid-functionalized complex **1P**. Fig. 3 displays the colour changes of the penta-hydrated form, **1P·5H$_2$O**, observed during two different drying processes (heating at 100 °C or vacuum at 23 °C). The **1P·5H$_2$O** complex is initially orange and exhibits a yellow emission centred at 585 nm devoid of any vibronic progression (Fig. 3(b) and the green spectrum in Fig. 4). This band is assigned to the ^{3}MMLCT emission derived from effective intermolecular Pt···Pt

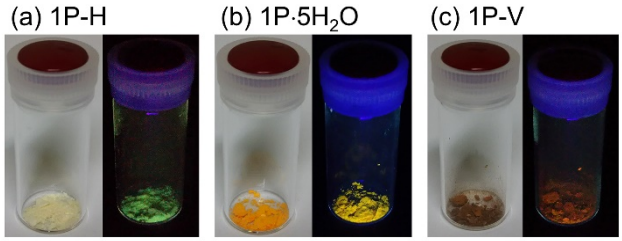

Fig. 3. Bright field and luminescence images of (a) heat-dried **1P-H**, (b) **1·5H$_2$O**, and (c) vacuum-dried **1P-V**.

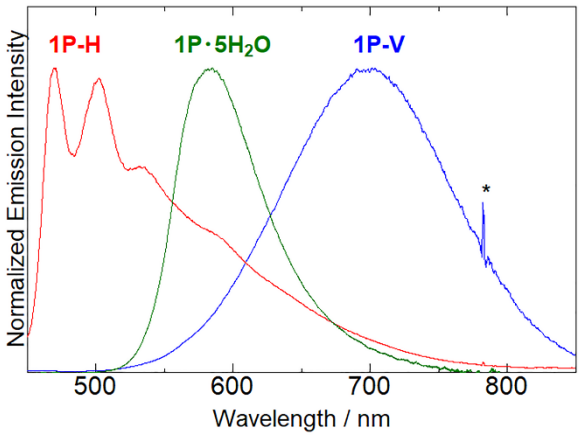

Fig. 4. Emission spectra of **1P·5H$_2$O**, **1P-H**, and **1P-V** in the solid state at 293 K (λ_{ex} = 400 nm). The sharp peak marked by the asterisk is a spectrofluorometer artefact.

interactions, as discussed above. Interestingly, the colour of the powder sample changed remarkably and became pale yellow upon heating at 100 °C (**1P-H**, Fig. 3(a)), while the sample dried under vacuum at room temperature was reddish-brown in colour (**1P-V**, Fig. 3(c)). Contrasting results were also observed in the luminescence photographs, spectra, and lifetime. The heated sample **1P-H** exhibited a blue-green emission centred at 469 nm with vibronic progression (Fig. 3(a) and the red spectrum in Fig. 4), whereas a dark-red emission centred at 701 nm was observed for the vacuum-dried sample (Fig. 3(c) and the blue spectrum in Fig. 4). Similar difference in the luminescence spectra were also observed even at 77 K (Fig. S3). The emission lifetime of **1P-H** was estimated to be significantly longer (13 μs) than that of the other two (130 and 437 ns for **1P·5H$_2$O** and **1P-V**, Fig. S4). The completely different colours, emissions, and lifetimes observed for **1P-H** and **1P-V** suggest that the original penta-hydrated **1P·5H$_2$O** can be transformed into the different less-hydrated (or anhydrous) phases. It is well known that the emission energy of a 1-D stacked Pt(II) complex strongly depends on the strength of intermolecular Pt···Pt interactions;[15] *i.e.*, stronger Pt···Pt interactions lower the MMLCT emission energy. Judging by the emission energies (wavelengths) observed for **1P-V** and **1P-H**, the intermolecular Pt···Pt interactions in **1P·5H$_2$O** are enhanced by vacuum drying, whereas they are significantly reduced by heat-drying. In fact, the emission spectrum of **1P-H** is qualitatively in agreement with that observed for **1P** in dilute aqueous solution (Fig. S5). These spectroscopic data indicate that the intermolecular Pt···Pt interactions in the heat-dried sample **1P-H** are as negligible as they are in dilute solution. The two different dried forms, **1P-H** and **1P-V**, are re-transformed into the original penta-hydrated **1P·5H$_2$O** by exposure to saturated water vapour at 293 K for several days (Fig. S6).

To clarify the origins of these different colours and the emission changes observed for **1P·5H$_2$O**, PXRD experiments were conducted under a variety of conditions. Figs. 5(a) and (b) reveal the dependences of the PXRD patterns of **1P-H** and **1P-V** on relative humidity (RH), respectively. As expected from the remarkable colour and emission changes observed for **1P·5H$_2$O**, the two samples exhibited very different diffraction patterns to that of the original penta-hydrated **1P·5H$_2$O**. It is noteworthy that the PXRD pattern of **1P-H** is in qualitative agreement with that simulated for anhydrous **1P**. In contrast, the pattern observed for **1P-V** was different to that of **1P-H**. These contrasting PXRD patterns clearly indicate that **1P·5H$_2$O** "recognizes" the drying process. On the other hand, the original **1P·5H$_2$O** was recovered by exposing the two different dried samples to water vapour. Although the PXRD pattern of **1P-H** hardly changed at relative humidity below 67% RH, as shown in Fig. 5(a), the two characteristic peaks below 5 degrees are clearly observed above 83% RH. Above 91% RH, the diffraction peaks corresponding to **1P-H** are completely absent and a pattern almost identical to that simulated for **1P·5H$_2$O** is observed. This result is also supported by the water-vapour adsorption isotherm of **1P-H**; that is, water

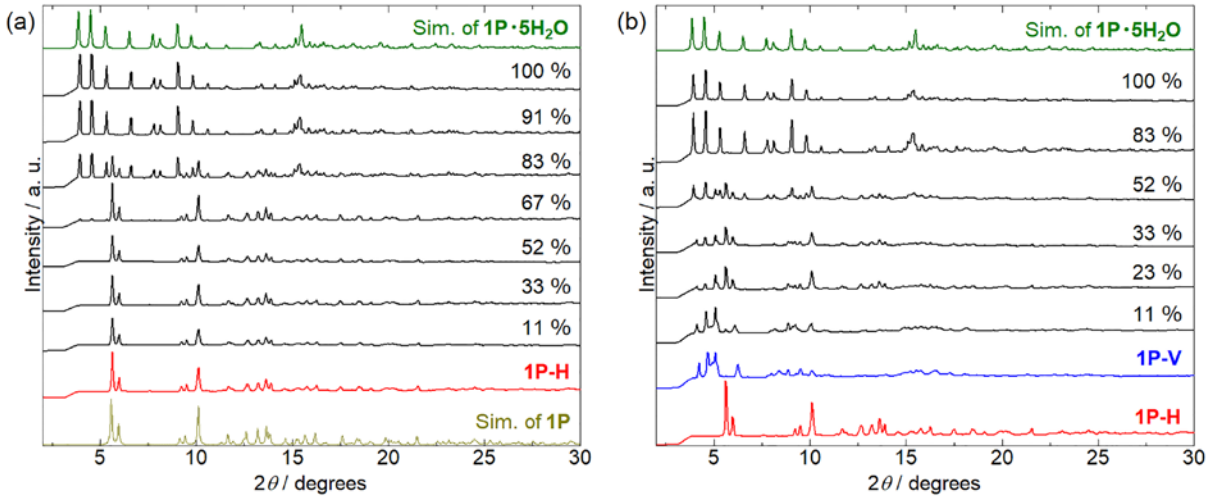

Fig. 5. Relative humidity dependences of PXRD patterns of (a) **1P-H**, and (b) **1P-V** at 293 K (λ= 0.88568 Å). The top green lines and the bottom brown line in the panel (a) are the simulations of **1P·5H$_2$O** and **1P**, respectively.

vapour is hardly adsorbed below 80% RH, but it is adsorbed above 80% RH to form **1P·5H$_2$O** (Fig. S7). As shown in Fig. 5(b), similar PXRD changes are observed for vacuum-dried **1P-V**, but there are several noteworthy differences. Although the pattern of **1P-H** hardly changed below 67% RH, as mentioned above, the pattern of **1P-V** changed at 23% RH, at which point peaks resembling those of **1P-H** are observed in addition to the original **1P-V** peaks. With further increases in relative humidity, the two characteristic peaks corresponding to **1P·5H$_2$O** (below 5 degrees) are clearly observed at 52% RH, and an almost identical pattern to that simulated for **1P·5H$_2$O** is observed above 83% RH. This two-step change in the PXRD pattern of **1P-V** is also supported by its water-vapour adsorption isotherm in which a two-step vapour uptake process is observed, one below 20% RH and the other above 60% RH (Fig. S7). In other words, the reason why the vacuum-dried **1P-V** exhibits a two-step structural transformation at a lower relative humidity during the recovery of the original penta-hydrated **1P·5H$_2$O** form, and **1P-H** does not, is associated with

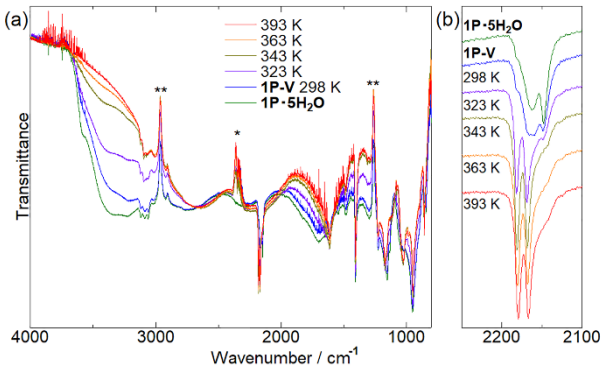

Fig. 6. Temperature dependence of the IR spectrum of **1P-V** in the solid state under vacuum compared to the spectrum of **1P·5H$_2$O** in air (green line). (a) All measured region and (b) the magnified view at the region of ν(C≡N) stretching mode. Blue, purple, yellow, orange and red lines show the spectra taken at 298, 323, 343, 363, and 393 K, respectively. Peaks marked by single and double asterisks in (a) are due to CO_2 in air and the grease used to fix the sample pellet on the optical stage, respectively.

their different crystal structures. We also attempted to further dry **1P-V** by heating at 100°C to form **1P-H**; however, the PXRD pattern hardly changed during the heating process (Fig. S8), which clearly indicates that dehydration from the penta-hydrated **1P·5H$_2$O** is necessary to form the blue-green-emissive anhydrous **1P-H**.

Although we were unsuccessful in structurally analysing **1P-V**, IR spectroscopy provided valuable information about the differences between **1P-H** and **1P-V**. Fig. 6 displays IR spectra of **1P-V** at different temperatures. The spectrum of **1P-V** at 298 K is very similar to that of **1P·5H$_2$O**, suggesting that the removal of water molecules from the **1P·5H$_2$O** crystal under vacuum to form **1P-V** does not affect the dominant intermolecularly hydrogen-bonded structure of **1P·5H$_2$O**. Several remarkable changes were observed when the sample temperature was increased. The O-H stretching band of water molecules in the crystal, at 3300 cm^{-1}, gradually disappeared, consistent with the loss of water from **1P-V**. In addition, thermogravimetric (TG) analysis suggests that **1P-V** contains one water molecule per Pt(II) complex (*i.e.*, it is the mono-hydrated form, **1P·H$_2$O**) which is removed by heating to 363 K to give the anhydrous form (Fig. S9). It should be noted that the characteristic cyanide-ligand bands significantly changed upon heat-drying, as shown in Fig. 6(b). Two peaks assigned to C≡N vibrations are observed at 2148 and 2162 cm^{-1} for both **1P·5H$_2$O** and **1P-V**, whereas these peaks were observed at higher energies (2167 and 2179 cm^{-1}) at temperatures above 323 K. These higher-energy-shifted peaks are also observed at almost the same positions after cooling to room temperature under vacuum (Fig. S10). Hence, the remarkable shifts to higher energies observed for these C≡N vibrations indicate

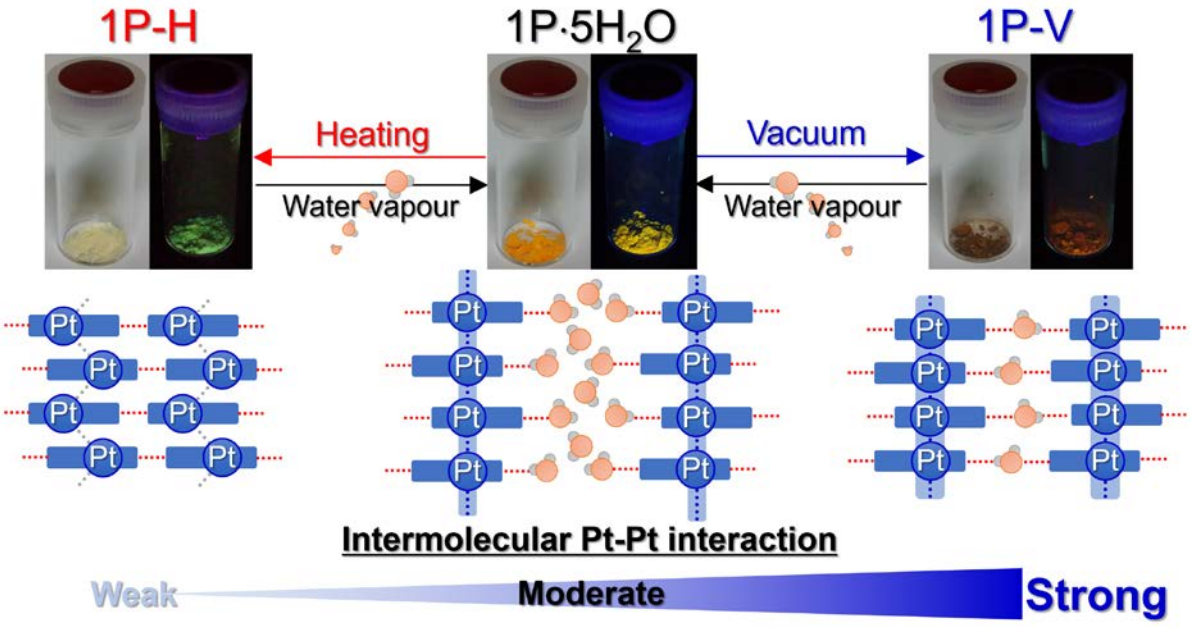

Scheme 2. Schematic diagram of the two-way vapochromism of **1**·5H$_2$O driven by heat- or vacuum-drying to form anhydrous **1P-H** and monohydrate **1P-V**.

that the intermolecularly hydrogen-bonded structure of **1P-V** changes significantly upon removal of water molecules from the crystal. A plausible origin for these C≡N-vibration shifts involves the formation of intermolecular hydrogen bonds to the phosphonic acid groups of the H_4dpbpy ligands. Interactions with highly acidic protons tend to increase C≡N vibrational energies owing to the donation of weakly antibonding electrons from the cyanide ligands. In fact, anhydrous **1P**, with tight intermolecular hydrogen bonds between the cyanide and phosphonic acid groups, exhibited a very similar spectrum to that of **1P-V** at 393 K (Fig. S10).

Plausible two-way vapochromism mechanism

As discussed in the previous section, penta-hydrated **1P·5H$_2$O** exhibits interesting vapochromism triggered by two different drying processes; *i.e.*, drying by heating or under vacuum at room temperature, as summarized in Scheme 2. In this section, we discuss the vapochromism mechanism in detail. Single crystal X-ray analyses clearly reveal that intermolecular Pt···Pt interactions are effective in **1P·5H$_2$O** but are negligible in anhydrous **1P** (Figs. 1 and 2). The **1P-H** sample obtained by heating **1P·5H$_2$O** at 100 ^{o}C was clearly characterized to be anhydrous **1P** by PXRD and TG (Fig. S9). This is the principal origin of the different colours observed for these two phases; that is, the effective Pt···Pt interactions stabilize the ^{3}MMLCT emissive state, resulting in the orange emission observed for **1P·5H$_2$O**. In contrast, the negligible intermolecular Pt···Pt interactions within anhydrous **1P** are probably the result of stronger intermolecular hydrogen bonds that are formed between the phosphonic acids and cyanide groups, as suggested by the IR spectra shown in Figs. 6 and S10. Such a tightly packed hydrogen-bonded structure requires relatively high RH (>80% RH) to trigger the structural transformation into the corresponding penta-hydrated phase. In contrast, the **1P-V** sample obtained by drying **1P·5H$_2$O** under vacuum at room temperature was characterized to be the monohydrate **1P·H$_2$O** by TG analysis (Fig. S9) and has a similar intermolecular hydrogen bonding network structure to that of **1P·5H$_2$O**, as suggested by IR spectroscopy (Fig. 6). Under vacuum at room temperature, the final hydrated water molecules are difficult to remove because of their strong intermolecular hydrogen bonds to the phosphonic acid and/or cyanide groups of complex **1P**. Although X-ray structure of **1P-V** was not determined yet, the reason why **1P-V** exhibits a ^{3}MMLCT emission at a longer wavelength than of **1P·5H$_2$O** is ascribable to a smaller hydration number that results in a more tightly packed structure with stronger intermolecular Pt···Pt interactions. Hence, we believe that the key factor that controls the interesting two-way vapochromic behaviour of **1P·5H$_2$O** is the presence (or absence) of the final hydrated water molecule that acts as an important supporter of the one-dimensionally stacked Pt(II) chain structure. When this final water molecule is removed, strong intermolecular hydrogen bonds are directly formed between the phosphonic acid and cyanide groups of adjacent complex molecules, resulting in the collapse of the one-dimensionally stacked Pt(II) chain structure.

Conclusions

In this work, we successfully synthesized luminescent Pt(II) complex **1P** bearing the phosphonic-acid-functionalized bipyridine ligand and showed that it exhibits interesting two-way vapochromic behaviour depending on the drying conditions. The luminescence colour of the penta-hydrated **1P·5H$_2$O** changed from orange to blue-green by drying at 100 ^{o}C, as it formed anhydrous **1P**. On the other hand, red luminescence was clearly observed upon vacuum-drying **1P·5H$_2$O** at room temperature to form mono-hydrated **1P·H$_2$O**. X-ray structural analyses clearly indicate that intermolecular Pt···Pt interactions are effective in **1P·5H$_2$O** while they are negligible in **1P**. IR spectroscopy reveals that the intermolecular hydrogen-bonding interactions around mono-hydrated **1P-V** are similar to those of the penta-hydrated form, whereas they significantly change upon removal of the final hydrated water molecule during the formation of anhydrous **1P**, in which adjacent molecules are directly hydrogen bonded. Further studies into the development of more intelligent vapochromic materials based on intermolecular hydrogen-bonding interactions are now in progress.

Acknowledgements

The authors thank Prof. Shin-ichiro Noro (Hokkaido Univ.) for his kind help with the IR spectroscopy. This study was supported by the Shimadzu Science Foundation, Shorai Science and Technology Foundation, Inamori Foundation, Murata Science Foundation, and Grants-in-Aid for Scientific Research (C) (No.26410063) and Artificial Photosynthesis (area No. 2406, No.15H00858), Soft Crystals (area No. 2903, No. JP17H06367) from MEXT, Japan.

Notes and references

1 O. S. Wenger, *Chem. Rev.*, 2013, **113**, 3686–3733 and references therein.
2 X. Zhang, B. Li, Z.-H. Chen, Z.-N. Chen, *J. Mater. Chem.*, 2012, **22**, 11427–11441 and references therein.
3 C. L. Exstrom, J. R. Sowa, Jr., C. A. Daws, D. Janzen, K. R. Mann, G. A. Moore, F. F. Stewart, *Chem. Mater.*, 1995, **7**, 15–17.
4 Y. Takashima, V. M. Martínez, S. Furukawa, M. Kondo, S. Shimomura, H. Uehara, M. Nakahama, K. Sugimoto, S. Kitagawa, *Nat. Commun.*, 2011, **2**, 168.
5 H. Hara, A. Kobayashi, S. Noro, H.-C. Chang, M. Kato, *Dalton Trans.*, 2011, **40**, 8012–8018.
6 T. Hayashi, A. Kobayashi, H. Ohara, M. Yoshida, T. Matsumoto, H.-C. Chang, M. Kato, *Inorg. Chem.*, 2015, **54**, 8905–8913.
7 X.-G. Liu, H. Wang, B. Chen, Y. Zou, Z.-G. Gu, Z. Zhao, L. Shen, *Chem. Commun.*, 2015, **51**, 1677–1680.
8 G. Mehlana, V. Chitsa, T. Mugadza, *RSC Adv.*, 2015, **5**, 88218–88233.
9 G. Kang, Y. Jeon, K. Y. Lee, J. Kim, T. H. Kim, *Cryst. Growth Des.*, 2015, **15**, 5183–5187.

10 A. Watanabe, A. Kobayashi, E. Saitoh, Y. Nagao, M. Yoshida, M. Kato, *Inorg. Chem.*, 2015, **54**, 11058–11060.
11 F. Drache, V. Bon, I. Senkovska, M. Adam, A. Eychmüller, S. Kaskel, *Eur. J. Inorg. Chem.*, 2016, **27**, 4483–4489.
12 H. Park, E. Kwon, H. Chiang, H. Im, K. Y. Lee, J. Kim, T. H. Kim, *Inorg. Chem.*, 2017, **56**, 8287–8294.
13 T. Miyano, I. Hisaki, N. Tohnai, *Chem. Lett.*, 2017, **46**, 225–227.
14 C. Zhang, L. Sun, Y. Yan. Y. Liu, Z. Liang, Y. Liu, J. Li, *J. Mater. Chem. C*, 2017, **5**, 2084–2089.
15 A. Kobayashi, M. Kato, *Eur. J. Inorg. Chem.*, 2014, 4469–4483 and references therein.
16 C. Jobbágy, A. Deák, *Eur. J. Inorg. Chem.* 2014, 4434–4449 and references therein.
17 R. Zhang, Z. Liang, A. Han, H. Wu, P. Du, W. Lai, R. Cao, *CrystEngComm*, 2014, **16**, 5531–5542.
18 J. Ni, J.-J. Kang, H.-H. Wang, X.-Q. Gai, X.-X. Zhang, T. Jia, L. Xu, Y.-Z. Pan, J.-J. Zhang, *RSC Adv.*, 2015, **5**, 65613–65617.
19 D. E. Janzen, K. R. Mann, *Dalton Trans.*, 2015, **44**, 4223–4237.
20 A. Deák, C. Jobbágy, G. Marsi, M. Molnár, Z. Szakács, P. Baranyai, *Chem. Eur. J.*, 2015, **21**, 11495–11508.
21 B. Jiang, J. Zhang, J.-Q. Ma, W. Zheng, L.-J. Chen, B. Sun, C. Li, B.-W. Hu, H. Tan, X. Li, H.-B. Yang, *J. Am. Chem. Soc.*, 2016, **138**, 738–741.
22 C.-J. Lin, Y.-H. Liu, S.-M. Peng, T. Shinmyozu, J.-S. Yang, *Inorg. Chem.*, 2017, **56**, 4978–4989.
23 P. Bolle, H. Serier-Brault, R. Génois, E. Faulques, A. Boulmier, O. Oms, M. Lepeltier, J. Marrot, A. Dolbecq, P. Mialane, R. Dessapt, *J. Mater. Chem. C*, 2016, **4**, 11392–11395.
24 T. Tsukamoto, R. Aoki, R. Sakamoto, R. Toyoda, M. Shimada, Y. Hattori, Y. Kitagawa, E. Nishibori, M. Nakano, H. Nishihara, *Chem. Commun.*, 2017, **53**, 9805–9808.
25 T. Ogoshi, Y. Shimada, Y. Sakata, S. Akine, T. Yamagishi, *J. Am. Chem. Soc.*, 2017, **139**, 5664–5667.
26 K. Yamaguchi, T. Murai, Y. Tsuchiya, Y. Miwa, S. Kutsumizu, T. Sasamori, N. Tokitoh, *RSC Adv.*, 2017, **7**, 18132–18135.
27 G. Iasilli, F. Martini, P. Minei, G. Ruggeri, A. Pucci, *Faraday Discuss.*, 2017, **196**, 113–129.
28 X. Zhu, P. Cui, S. Kilina, W. Sun, *Inorg. Chem.*, 2017, *in press.* (DOI: 10.1021/acs.inorgchem.7b01472)
29 T. Ohba, A. Kobayashi, H.-C. Chang, T. Kouyama, T. Kato, M. Kato, *Dalton Trans.*, 2014, **43**, 7514–7521.
30 J. Forniés, N. Giménez, S. Ibáñez, E. Lalinde, A. Martín, M. T. Moreno, *Inorg. Chem.*, 2015, **54**, 4351–4363.
31 H.-Y. Tang, Z. Chu, C.-P. Li, X.-M. Ren, C. Xue, W. Jin, *Dalton Trans.*, 2016, **45**, 10249–10255.
32 H. Ohara, T. Ogawa, M. Yoshida, A. Kobayashi, M. Kato, *Dalton Trans.*, 2017, **46**, 3755–3760.
33 T. Hasegawa, A. Kobayashi, H. Ohara, M. Yoshida, M. Kato, *Inorg. Chem.*, 2017, **56**, 4928–4936.
34 P. Kar, M. Yoshida, Y. Shigeta, A. Usui, A. Kobayashi, T. Minamidate, N. Matsunaga, M. Kato, *Angew. Chem. Int. Ed.*, 2017, **56**, 2345–2349.
35 Z. Lei, S.-S. Chang, Q.-M. Wang, Eur. J. *Inorg. Chem.*, 2017, *in press*. (DOI: 10.1002/ejic.201701012)
36 B. R. Varju, J. S. Ovens, D. B. Leznoff, *Chem. Commun.*, 2017, **53**, 6500–6503.
37 A. S. Sergeenko, J. S. Ovens, D. B. Leznoff, *Inorg. Chem.*, 2017, **56**, 7870–7881.
38 A. Kobayashi, S. Oizumi, Y. Shigeta, M. Yoshida, M. Kato, *Dalton Trans.*, 2016, **45**, 17485–17494.
39 M. Kato, S. Kishi, Y. Wakamatsu, Y. Sugi, Y. Osamura, T. Koshiyama, M. Hasegawa, *Chem. Lett.*, 2005, **34**, 1368-1369.
40 A. Kobayashi, Y. Fukuzawa, H.-C. Chang, M. Kato, *Inorg. Chem.*, 2012, **51**, 7508–7519.
41 Y. Shigeta, A. Kobayashi, T. Ohba, M. Yoshida, T. Matsumoto, H.-C. Chang, M. Kato, *Chem. Eur. J.*, 2016, **22**, 2682–2690.
42 G. Gilli, P. Gilli, *The Nature of the Hydrogen Bond: outline of a comprehensive hydrogen bond theory*, Oxford university press, 2009.
43 G. R. Desiraju, T. Steiner, *The weak hydrogen bond: in structural chemistry and biology,* Oxford university press, 1999.
44 T. J. Wadas, Q.-M. Wang, Y.-j. Kim, C. Flaschenreim, T. N. Blanton, R. Eisenberg, *J. Am. Chem. Soc.*, 2004, **126**, 16841–16849.
45 A. Han, P. Du, Z. Sun, H. Wu, H. Jia, R. Zhang, Z. Liang, R. Cao, R. Eisenberg, *Inorg. Chem.*, 2014, **53**, 3338–3344.
46 N. Kitani, N. Kuwamura, T. Tsuji, K. Tsuge, T. Konno, *Inorg. Chem.*, 2014, **53**, 1949–1951.
47 N. Komiya, M. Okada, K. Fukumoto, S. Iwata, T. Naota, *Dalton Trans.*, 2014, **43**, 10074–10085.
48 N. Yoshinari, T. Shimizu, K. Nozaki, T. Konno, *Inorg. Chem.*, 2016, **55**, 2030–2036.
49 K. Ohno, H. Tanuma, Y. Kusano, S. Kaizaki, A. Nagasawa, T. Fujihara, *Dalton Trans.*, 2017, **46**, 7612–7618.
50 J. Kuwabara, K. Yamaguchi, K. Yamawaki, T. Yasuda, Y. Nishimura, T. Kanbara, *Inorg. Chem.*, 2017, **56**, 8726–8729.
51 M. Li, Q. Zhang, H. He, J.-R. Wang, X. Mei, *J. Mater. Chem. C*, 2017, **5**, 5970–5976.
52 A. Avshu, A. W. Parkins, *J. Chem. Res. Synop.* 1984, 245.
53 M. R. Norris, J. J. Concepcion, C. R. K. Glasson, Z. Fang, A. M. Lapides, D. L. Ashford, J. L. Templeton, T. J. Meyer, *Inorg. Chem.*, 2013, **52**, 12494–12501.
54 *CrysAlis PRO*, Oxford Diffraction Ltd, Yarnton, England, **2009**. *CrystalClear*: Molecular Structure Corporation: Orem, UT, **2001**.
55 *SIR-2004*: M. C. Burla, R. Caliandro, M. Camalli,B. Carrozzini, G. L. Cascarano, L. De Caro, C. Giacovazzo, G. Polidori, R. Spagna, *J. Appl. Crystallogr.*, 2005, **38**, 381. *SIR-2014*: M. C. Burla, R. Caliandro, B. Carrozzini, G. L. Cascarano, C. Giacovazzo, M. Mallamo, A. Mazzone, G. Polidori, *J. Appl. Cryst.*, 2015, **48**, 306.
56 *SHELXL2013*: G. M. Sheldrick, *Acta Cryst.*, 2008, **A64**, 112–122.
57 *CrystalStructure 4.1*: Crystal Structure Analysis Package; Rigaku Corporation: Tokyo, Japan, 2000–2014.

